Received 5 July 2024; revised 25 August 2024; accepted 15 September 2024. Date of publication 19 September 2024; date of current version 3 October 2024.

Digital Object Identifier 10.1109/OJCOMS.2024.3464348

Multi-RIS Assisted Hybrid Beamforming Design for Terahertz Massive MIMO Systems

IBRAHIM YILDIRIM [1,2] (Member, IEEE), ASIL KOC [1] (Member, IEEE), ERTUGRUL BASAR [2] (Fellow, IEEE), AND THO LE-NGOC [1] (Life Fellow, IEEE)

[1]Department of Electrical and Computer Engineering, McGill University, Montreal, QC H1X 2E4, Canada

[2]Communications Research and Innovation Laboratory, Department of Electrical and Electronics Engineering, Koç University, 34450 Istanbul, Türkiye

CORRESPONDING AUTHOR: I. YILDIRIM (e-mail: ibrahim.yildirim@mcgill.ca)

The work of Ibrahim Yildirim was supported by the Scientific and Technological Research Council of Turkey (TÜBİTAK) under Grant BİDEB 2214. This work was supported in part by the Natural Sciences and Engineering Research Council of Canada (NSERC), InterDigital Canada, and Prompt Quebec under an NSERC Alliance Grant.

ABSTRACT This paper presents an innovative approach for terahertz (THz) band communications, utilizing reconfigurable intelligent surfaces (RISs) to implement an angular-based hybrid beamforming (AB-HBF). This study examines two significant THz channel scenarios with cost-efficient solutions utilizing RISs to enhance performance. The first scenario ensures reliable communication in the presence of obstacles blocking the direct path, where RISs offer an alternative transmission path. The second scenario leverages multiple-RIS in line-of-sight dominant or sparse environments to increase the rank of the channel matrix, consequently improving the achievable rate. By introducing an innovative HBF design for multiple-RIS-assisted THz massive MIMO systems, a three-stage design is proposed based on a geometry-based THz channel model. This design encompasses the transmit and receive radio frequency (RF) beamformers, transmit/receive baseband (BB) precoder/combiner, and RIS phase shift matrix. A particle swarm optimization-based solution is employed to design the RIS phase reflections. This design methodology is extended to the multiple-RIS-aided scenario, optimizing the phase shift matrices of each RIS. We also provide sub-connected AB-HBF configuration by offering a remarkable reduction in the total number of phase shifters compared to the fully-connected AB-HBF. Additionally, a deep learning-based phase shift design is incorporated to effectively optimize the RIS configurations, significantly reducing the computational time required for system calibration in dynamic THz environments. Extensive numerical experiments demonstrate the significant enhancement in the achievable rate of THz AB-HBF systems by incorporating RISs, mitigating the wireless propagation disruptions as well as reducing hardware cost/complexity and power consumption for massive MIMO systems.

INDEX TERMS Hybrid beamforming, terahertz band, massive MIMO, low CSI overhead, reconfigurable intelligent surface.

I. INTRODUCTION

IN the envisioned future of wireless communication systems, the utilization of a substantially large spectrum at high frequencies is of utmost importance to facilitate the provision of unparalleled performance for unique applications such as holographic teleportation, autonomous systems, extended reality, and digital twins [1]. To meet these demands, it is crucial to enhance the existing wireless spectrum bands below 6 GHz and in the millimeter wave (mmWave) range by migrating towards the higher frequency terahertz (THz) bands, which offer abundant bandwidth [2]. THz communications offer high-speed transmission capabilities and potential applications in various fields such as sensing, imaging, and localization [3]. The THz band, ranging from 0.1 to 10 THz, is considered crucial for next-generation wireless systems due to its ability to support high-speed transmission and accommodate the increasing wireless data traffic [4]. However, the free space propagation

© 2024 The Authors. This work is licensed under a Creative Commons Attribution-NonCommercial-NoDerivatives 4.0 License.
For more information, see https://creativecommons.org/licenses/by-nc-nd/4.0/

modality of THz communications poses challenges like dependence on atmospheric conditions, rapid beam divergence, and the line-of-sight nature of links, which can restrict the applications of THz communication systems [5]. While the mmWave transmission is already established as a fundamental component of fifth-generation (5G) and beyond communication systems, the introduction of promising technologies such as massive multiple-input multiple-output (MIMO) and reconfigurable intelligent surface (RIS) has been undertaken to tackle the challenges arising from high path loss and vulnerability to blockage at the higher frequencies [6], [7], [8], [9]. RISs, composed of low-cost and passive reflecting elements, have recently garnered significant attention from both academia and industry owing to their capacity-enhancing capabilities and their potential to improve the transmission performance of wireless communication systems.

By leveraging the massive MIMO technique, which employs a large number of antennas at both the transmitter and receiver sides, it becomes possible to exploit the abundant spatial degrees of freedom and achieve substantial capacity enhancements. The high number of antennas allows for increased spatial multiplexing, enabling simultaneous transmission of multiple data streams, thereby significantly boosting the capacity of the system. In THz communications, the integration of massive MIMO systems, which employ beamforming technologies to generate highly directional beams with high gain, offers a practical solution to counteract propagation loss [10]. In terms of cost efficiency, the hybrid beamforming (HBF) architecture has emerged as an appealing choice for massive MIMO systems [11], [12]. By combining the advantages of both analog and digital processing, the HBF architecture achieves a comparable performance to digital beamforming while exhibiting significantly lower hardware cost and power consumption [13], [14]. Moreover, a previous study [15] introduced the angular-based HBF (AB-HBF) technique as a solution that not only minimizes hardware cost and complexity by employing a limited number of radio frequency (RF) chains but also reduces the channel state information (CSI) overhead by designing the RF stage based on slow time-varying CSI, specifically angular information. Consequently, the reduced-size effective CSI is employed in the baseband (BB) stage design. Additionally, AB-HBF also exhibits considerably lower computational complexity compared to conventional single-stage fully digital beamforming approaches.

In traditional HBF systems, designed as a fully-connected HBF (FC-HBF) structure, each RF chain is connected to all antenna elements. Therefore, the FC-HBF systems allow each RF chain to benefit from the complete beamforming capability of all antenna elements within the antenna array. In order to mitigate the cost/complexity associated with the elevated number of RF chains, the sub-connected HBF (SC-HBF) structure has been introduced in [16]. This alternative design enables an arrangement, where a specific RF chain is connected to a carefully chosen subset of antenna elements. Obviously, the SC-HBF structure does not benefit from full beamforming capability for all RF chains, the dynamic selection capability of sub-antenna-arrays provides flexible design opportunities as well as a reduced number of phase shifters [17].

A. PRIOR WORKS

The mmWave/THz channels exhibit sparsity and strong directivity, primarily consisting of a dominant line-of-sight (LoS) cluster and several weaker non-line-of-sight (NLoS) clusters, especially when massive antenna elements are employed [7], [18], [19]. Furthermore, RISs can also be considered as an efficient tool to enhance the rank of the MIMO channel matrix, mitigate multipath fading, and optimize spatial multiplexing performance by adjusting the RIS-assisted communication channel through the design of the RIS phase shift matrix [20], [21], [22].

The integration of RIS and massive MIMO hybrid beamforming systems in THz frequencies has emerged as an appealing area of investigation, as evidenced by recent scholarly attention [23], [24], [25], [26]. In [23], the authors introduce an HBF technique for multi-hop communication networks assisted by RIS in the THz frequency range, focusing on enhancing coverage range, and employs deep reinforcement learning to jointly optimize the digital beamforming matrix at the base station (BS) and analog beamforming matrices at the RIS to mitigate propagation loss. The study presented in [24] introduces a RIS-based HBF architecture for THz communication, leveraging the energy-efficient properties of the RIS in place of the power-consuming phased array for analog beamforming while also optimizing the hybrid precoding matrix to maximize the sum-rate of the users. In [25], the authors introduce a low-complexity beam training and HBF approach for THz multi-user massive MIMO systems utilizing RIS. Through numerical analysis, they illustrate that integrating RIS results in significant performance improvements compared to systems without RIS. The work [26] presents a comprehensive study on the development of a wideband HBF solution for the joint radar communication architecture in ultra-massive MIMO systems operating in the THz frequency range. They also propose model-based and model-free HBF techniques depending on both CSI and channel covariance matrix. In [27], the authors investigate the uplink multi-access of THz communication using multi-hop RIS in environments with correlated channels. This research focuses on improving the data rate for a specific user while managing interference from other users, and on enhancing the overall combined data rate of the system. In [28], the authors examine a UAV equipped with an active RIS in the THz band, focusing on optimizing a joint power allocation and active RIS precoding matrix to maximize the sum rate for a scenario involving only RIS-reflected paths among a cellular user and multiple device-to-device (D2D) links. Their findings demonstrate that the proposed active RIS-aided scheme outperforms traditional passive RIS

and multi-antenna amplify-and-forward relaying methods, achieving superior sum rate results.

In summary, to the best of our knowledge, HBF designs in the existing THz communications literature have been mostly made by performing analog beamforming in RIS instead of a transmitter. Moreover, angular-based HBF-based solutions have not yet been considered in RIS-based THz band systems. Consequently, there remains a demand for a power and cost-efficient HBF design that enhances performance and spatial multiplexing gain, effectively exploiting the advantageous features of RIS and massive MIMO systems.

B. CONTRIBUTIONS

In this paper, we introduce two innovative angular-based HBF designs for single and multiple-RIS-aided THz massive MIMO systems, employing low CSI overhead. We examine two critical scenarios commonly encountered in THz channels and present cost and energy-efficient solutions utilizing RISs to enhance system performance as well as reduce CSI overhead. Within this context, our major contributions are summarized below:

- First, we focus on a scenario in the presence of obstacles blocking the direct path between the transmitter and receiver, where an RIS offers an alternative transmission path, maintaining reliable communication. At mmWave frequencies, both line-of-sight (LoS) and non-line-of-sight (NLoS) paths play a significant role. However, in the THz band, the NLoS paths have minimal impact on the received power, resulting in a communication scenario characterized by LoS dominance and NLoS assistance at THz frequencies. If the LoS link is blocked, providing the transmission over the weak NLoS channels will threaten reliable communication. In this case, while it is aimed to provide reliable communication by using an LoS RIS-assisted link, NLoS channels efficiently will be used in the transmission to increase the performance of the system by proposing the proper AB-HBF designs.
- Another major challenge in THz channels lies in efficiently transmitting multiple data streams along orthogonal paths, particularly in scenarios where a reliable LoS channel is present between the transmitter and receiver. In this scenario, we explore leveraging multiple-RIS in LoS dominant and sparse environments to transmit multiple data streams over orthogonal links, consequently aiming to improve the achievable rate performance as well as the rank of the channel matrix. Through the introduction of an innovative HBF design for multi-RISs-assisted THz massive MIMO systems, the overarching goal of attaining enhanced spatial multiplexing gain is achieved with the effective utilization of NLoS paths, as well as the RIS-assisted path during the transmission.
- By utilizing a 3D geometry-based THz channel model, we propose a three-stage design for the RIS-aided HBF system: *i)* The transmit and receive RF beamformers, *ii)* the transmit/receive BB precoder/combiner, and *iii)* RIS phase shift matrix design. Here, the transmit and receive RF beamformers are designed based on the slow time-varying angle-of-arrival/angle-of-departure (AoA/AoD) information of the channel, while the BB precoder and combiner exploit the reduced-size effective channel observed at the BB stage. Furthermore, we employ particle swarm optimization (PSO) to design the RIS phase reflection matrix, aiming to maximize the achievable rate of THz massive MIMO systems. Then, we extend this design methodology to multiple-RIS-aided scenarios to optimize the phase shift matrices of each RIS.
- As a natural extension of our proposed system, we extend the traditional FC-HBF-based design to the SC-HBF design for the RIS-enabled THz AB-HBF system. This new approach aims to notably reduce hardware and analog beamforming implementation costs compared to FD-HBF-based THz mMIMO systems. By comparing with FC-HBF systems, we demonstrate the potential for improved adaptability, efficiency, and cost-effectiveness in RIS-enabled THz communication systems, highlighting the advantages of the SC-HBF structure.
- We also introduce a deep learning (DL)-based approach for phase shift design, specifically tailored for RIS-aided systems. Leveraging a convolutional neural network (CNN) trained via PSO, this method dynamically configures optimal phase settings to maximize system performance under variable channel conditions. This deep learning framework allows for an adaptive and efficient computation of RIS phase shifts, significantly reducing the time and computational resources required compared to traditional optimization methods.
- Through extensive numerical experiments, we demonstrate the significant enhancement in achievable rate performance of the THz AB-HBF systems by incorporating RISs, which effectively alleviate the disruptive effects of the wireless propagation environment. The proposed AB-HBF techniques utilize a considerably smaller number of RF chains for connecting the RF-stage and BB-stage compared to the number of antennas. This not only reduces the hardware cost/complexity and power consumption for mMIMO systems with large antenna arrays but also employs reduced-size effective intended channel matrices in the AB-HBF design, replacing the full-size instantaneous CSI. This approach significantly reduces the overhead associated with channel estimation.

C. ORGANIZATION

The rest of this paper is organized as follows. The system and channel models are described in Section II. The problem formulations for the proposed AB-HBF techniques are introduced in Section III. Then, we develop the RF beamformers, BB precoder/combiner and phase shift matrix solutions in Section IV. The extensive illustrative results are

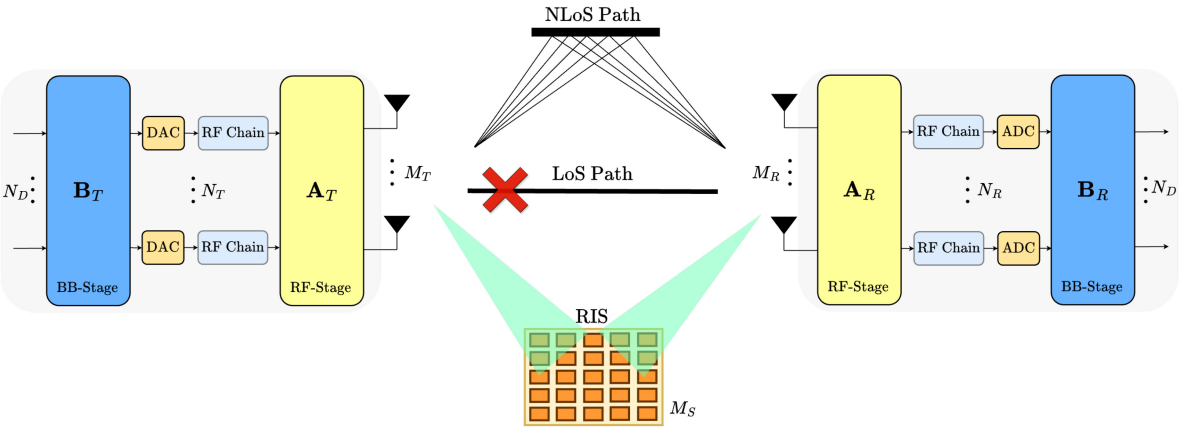


FIGURE 1. RIS-assisted hybrid THz massive MIMO system model.

presented in Section V. Finally, the paper is concluded in Section VI.

II. SYSTEM AND CHANNEL MODEL

In this section, we introduce the system and channel models of the single and multiple-RIS-assisted AB-HBF schemes for THz massive MIMO systems, elucidating their underlying operational principles.

A. SINGLE RIS-AIDED TRANSMISSION

A hybrid THz massive MIMO architecture is considered by incorporating an RIS, as depicted in Fig. 1. The system configuration consists of a single RIS positioned between the transmitter (Tx) and receiver (Rx). Both the Tx and Rx, along with the RIS, are equipped with half-wavelength spaced uniform rectangular arrays (URAs). The RIS is equipped with $M_S = M_{S_x} \times M_{S_y}$ dynamically adjustable reflecting elements, while the Tx and Rx possess $M_T = M_{T_x} \times M_{T_y}$ and $M_R = M_{R_x} \times M_{R_y}$ antennas, respectively. The digital BB precoder (B_T) and analog RF beamformer (A_T) are employed at the Tx to transmit N_D data streams, utilizing N_T RF chains. At the Rx, the received signal is processed through the analog RF beamformer (A_R) and digital baseband combiner (B_T), linked to N_R RF chains. The constraint $N_D \leq \min(N_T, N_R)$ limits the number of data streams, and the number of RF chains is significantly smaller than the count of transmit and receive antennas with $N_T \ll M_T$ and $N_R \ll M_R$ from exploiting the advantages of HBF systems.

The precoded and transmitted signal $\tilde{x} \in \mathbb{C}^{M_T}$ from the Tx is formulated as:

$$\tilde{x} = A_T B_T x, \tag{1}$$

where $A_T \in \mathbb{C}^{M_T \times N_T}$ denotes the transmit RF beamformer, $B_T \in \mathbb{C}^{N_T \times N_D}$ denotes the BB precoder and $x \in \mathbb{C}^{N_D}$ stands for the data symbol vector, which ensures $\mathbb{E}\{xx^H\} = I_{N_D}$. Furthermore, the transmitted power P_{T_x} is subject to a power constraint, denoted by $\mathbb{E}\{\|\tilde{x}\|_2^2\} \leq P_{T_x}$.

In the considered communication system, the data can be transmitted over three distinct channels, namely the LoS and NLoS channels between the Tx and Rx, along with the channel assisted by the RIS. Here, the LoS and NLoS channel between the Tx and Rx are respectively denoted by $H_{\text{LoS}} \in \mathbb{C}^{M_R \times M_T}$ and $H_{\text{NLoS}} \in \mathbb{C}^{M_R \times M_T}$, while the RIS-assisted link comprises two components: $H_{\text{Tx-RIS}} \in \mathbb{C}^{M_S \times M_T}$ represents the channel matrix from the Tx to the RIS, and $H_{\text{Rx-RIS}} \in \mathbb{C}^{M_R \times M_S}$ represents the channel matrix from the RIS to the Rx. Moreover, $\Theta = \text{diag}(e^{j\Omega_1}, \ldots, e^{j\Omega_{M_S}}) \in \mathbb{C}^{M_S \times M_S}$ corresponds to the phase reflection matrix of the RIS, where Ω_i denotes the phase shift introduced by the ith reflecting element of the RIS for $i = 1, \ldots, M_S$. Then, the received signal from the LoS, NLoS and RIS-assisted paths at the Rx is expressed as

$$\begin{aligned} r &= H\tilde{x} + n = (H_{\text{LoS}} + H_{\text{NLoS}} + H_{\text{RIS-Rx}}\Theta H_{\text{Tx-RIS}})\tilde{x} + n \\ &= (H_{\text{LoS}} + H_{\text{NLoS}} + H_{\text{RIS-Rx}}\Theta H_{\text{Tx-RIS}})A_T B_T x + n, \end{aligned} \tag{2}$$

where $H = H_{\text{LoS}} + H_{\text{NLoS}} + H_{\text{RIS-Rx}}\Theta H_{\text{Tx-RIS}} \in \mathbb{C}^{M_R \times M_T}$ denotes the end-to-end channel matrix, while $n \sim \mathcal{CN}(0, \sigma_n^2 I_{M_R})$ denotes the complex Gaussian noise vector.

With $\boldsymbol{\mathcal{H}} = A_R H A_T \in \mathbb{C}^{N_R \times N_T}$ being the effective channel matrix seen from the BB stages, the combined signal after the digital BB combiner is expressed as

$$\tilde{r} = B_R \boldsymbol{\mathcal{H}} B_T x + B_R A_R n, \tag{3}$$

where $A_R \in \mathbb{C}^{N_R \times M_T}$ and $B_R \in \mathbb{C}^{N_D \times N_R}$ denotes the receive RF beamformer and the BB combiner, respectively.

The primary objective of our study is to effectively design A_T, B_T, A_R, B_R and Θ. This design aims to maximize the achievable rate of the system, which is represented by

$$\max_{\{A_T, A_R, B_T, B_R, \Theta\}} \quad R = \log_2 \det\left(I_{N_D} + R_v^{-1} \tilde{\boldsymbol{\mathcal{H}}} \tilde{\boldsymbol{\mathcal{H}}}^H\right), \tag{4a}$$

$$\text{s.t. } \tilde{\boldsymbol{\mathcal{H}}} = B_R \boldsymbol{\mathcal{H}} B_T \in \mathbb{C}^{M_R \times M_T}, \tag{4b}$$

$$\boldsymbol{\mathcal{H}} = A_R H A_T \in \mathbb{C}^{N_R \times N_T}, \tag{4c}$$

$$|A_T(i,j)| = \frac{1}{\sqrt{M_T}}, |A_R(i,j)| = \frac{1}{\sqrt{M_R}}, \forall (i,j), \tag{4d}$$

$$\mathbb{E}\{\|\tilde{\mathbf{x}}\|_2^2\} = \text{tr}\left(B_T^H A_T^H A_T B_T\right) \leq P_{T_x}, \tag{4e}$$

The covariance matrix of the noise $v = B_R A_R n$ is denoted as $R_v = \sigma_n^2 B_R A_R A_R^H B_R^H$. In order to satisfy the implementation requirements of the RF beamformer, the constant-modulus constraint in (4d) is ensured due to the utilization of phase shifters.

In this section, we also introduce a widely adopted statistical channel model known as the Saleh-Valenzuela (S-V) channel model [29], which finds extensive application in massive MIMO systems. By leveraging the implementation of a large number of antenna elements, sparsity and strong directivity are typically obtained in the THz channel, characterized by a dominant LoS cluster and multiple weaker NLoS clusters. Hence, by considering the URA structure, the channel matrix can be written as

$$H = \underbrace{\frac{z_0}{\sqrt{\alpha \tau_0^{n_0}}} \boldsymbol{a}_R^T\left(\gamma_{x,R}^{\mathrm{LoS}}, \gamma_{y,R}^{\mathrm{LoS}}\right) \boldsymbol{a}_T\left(\gamma_{x,T}^{\mathrm{LoS}}, \gamma_{y,T}^{\mathrm{LoS}}\right)}_{H_{\mathrm{LoS}}} + \underbrace{\sum_{q=1}^{Q} \frac{z_q}{\sqrt{\alpha \tau_q^{n}}} \boldsymbol{a}_R^T\left(\gamma_{x,R}^{\mathrm{NLoS},q}, \gamma_{y,R}^{\mathrm{NLoS,q}}\right) \boldsymbol{a}_T\left(\gamma_{x,T}^{\mathrm{NLoS},q}, \gamma_{y,T}^{\mathrm{NLoS},q}\right)}_{H_{\mathrm{NLoS}}} + H_{\text{RIS-Rx}} \Theta H_{\text{Tx-RIS}} \tag{5}$$

where $z_0 \sim \mathcal{CN}(0,1)$ and $z_q \sim \mathcal{CN}(0, 1/Q)$ respectively stand for the complex path gain of the LoS channel and q^{th} $(q = 1, \ldots, Q)$ path of the NLoS channel with Q being the total number of NLoS paths, the reference path loss is denoted in dB as $\alpha = 32.4 + 20\log_{10}(f_c)$, η_0 and η respectively represents the path loss exponents of LoS and NLoS paths. Moreover, τ_0 and τ_q respectively represent the distance of LoS path and q^{th} NLoS path from the Tx and Rx, where $q = 1, \ldots, Q$. Here, the RIS-assisted sub-channels for the Tx-RIS and RIS-Rx links are respectively defined as

$$\begin{aligned} H_{\text{Tx-RIS}} &= \frac{z_{\text{Tx-RIS}}}{\sqrt{\alpha \tau_{\text{Tx-RIS}}^{n_0}}} \boldsymbol{a}_R^T\left(\gamma_{x,R}^{\text{Tx-RIS}}, \gamma_{y,R}^{\text{Tx-RIS}}\right) \boldsymbol{a}_T\left(\gamma_{x,T}^{\text{Tx-RIS}}, \gamma_{y,T}^{\text{Tx-RIS}}\right), \\ H_{\text{RIS-Rx}} &= \frac{z_{\text{RIS-Rx}}}{\sqrt{\alpha \tau_{\text{RIS-Rx}}^{n_0}}} \boldsymbol{a}_R^T\left(\gamma_{x,R}^{\text{RIS-Rx}}, \gamma_{y,R}^{\text{RIS-Rx}}\right) \boldsymbol{a}_T\left(\gamma_{x,T}^{\text{RIS-Rx}}, \gamma_{y,T}^{\text{RIS-Rx}}\right) \end{aligned} \tag{6}$$

where $z_i \sim \mathcal{CN}(0,1)$ is the complex path gain, τ_i is the distance of the corresponding path for $i \in \{\text{Tx-RIS}, \text{RIS-Rx}\}$. The Tx/Rx array steering vector for considered URA geometry is obtained as

$$\boldsymbol{a}_i\left(\gamma_{x,i}^j, \gamma_{y,i}^j\right) = \left[1, e^{j2\pi d \gamma_{x,i}^j}, \ldots, e^{j2\pi d (M_{k_x}-1)\gamma_{x,i}^j}\right]^T \otimes \left[1, e^{j2\pi d \gamma_{y,i}^j}, \ldots, e^{j2\pi d \left(M_{k_y}-1\right)\gamma_{y,i}^j}\right]^T, \tag{7}$$

where $i \in \{T, R\}$, $j \in \{\text{LoS}, \text{NLoS}, \text{Tx-RIS}, \text{RIS-Rx}\}$, $k \in \{T, R, S\}$ and d is the inter-element spacing normalized by the wavelength. For the LoS paths, the coefficients reflecting the elevation and azimuth AoA (AoD) can be respectively calculated as $\gamma_{x,R}^j = \sin(\theta_R^j)\cos(\psi_R^j)$ $(\gamma_{x,T}^j = \sin(\theta_T^j)\cos(\psi_T^j))$ and $\gamma_{y,R}^j = \sin(\theta_R^j)\sin(\psi_R^j)$ $(\gamma_{y,T}^j = \sin(\theta_T^j)\sin(\psi_T^j))$, where θ_R^j (θ_T^j) and ψ_R^j (ψ_T^j) are respectively elevation and azimuth AoA (AoD) at the receive (transmit) node of each channel with $j \in \{\text{LoS}, \text{Tx-RIS}, \text{RIS-Rx}\}$.

TABLE 1. Angular parameters of q^{th} the NLoS channel for $q = 1, \ldots, Q$.

AoA Parameters		AoD Parameters	
$\theta_{R,q}^{\text{NLoS}}$	Mean elevation	$\theta_{T,q}^{\text{NLoS}}$	Mean elevation
$\delta_{R,q}^{\text{NLoS},\theta}$	Elevation spread	$\delta_{T,q}^{\text{NLoS},\theta}$	Elevation spread
$\psi_{R,q}^{\text{NLoS}}$	Mean azimuth	$\psi_{T,q}^{\text{NLoS}}$	Mean azimuth
$\delta_{R,q}^{\text{NLoS},\psi}$	Azimuth spread	$\delta_{T,q}^{\text{NLoS},\psi}$	Azimuth spread

By considering the AoA/AoD mean and spread parameters defined in Table 1, the coefficients reflecting the elevation and azimuth AoA (AoD) for the q^{th} path of the NLoS channel can be respectively calculated as $\gamma_{x,R}^{\text{NLoS},q} = \sin(\theta_{R,q}^{\text{NLoS}})\cos(\psi_{R,q}^{\text{NLoS}})$ $(\gamma_{x,T}^{\text{NLoS},q} = \sin(\theta_{T,q}^{\text{NLoS}})\cos(\psi_{T,q}^{\text{NLoS}}))$ and $\gamma_{y,R}^{\text{NLoS},q} = \sin(\theta_{R,q}^{\text{NLoS}})\sin(\psi_{R,q}^{\text{NLoS}})$ $(\gamma_{y,T}^{\text{NLoS},q} = \sin(\theta_{T,q}^{\text{NLoS}})\sin(\psi_{T,q}^{\text{NLoS}}))$, where θ_R^j $(\theta_{T,q}^{\text{NLoS}})$ and $\psi_{R,q}^{\text{NLoS}}$ $(\psi_{T,q}^{\text{NLoS}})$ are respectively elevation and azimuth AoA (AoD) at the receive (transmit) node with $q = 1, \ldots, Q$.

In order to decompose the slow and fast time-varying components of each channel, the end-to-end channel in (5) can be rewritten as

$$H = \underbrace{\Phi_R G \Phi_T}_{H_{\text{LoS}}+H_{\text{NLoS}}} + \underbrace{\phi_R^{\text{RIS-Rx}} G_{\text{RIS-Rx}} \phi_T^{\text{RIS-Rx}}}_{H_{\text{RIS-Rx}}} \Theta \underbrace{\phi_R^{\text{Tx-RIS}} G_{\text{Tx-RIS}} \phi_T^{\text{Tx-RIS}}}_{H_{\text{Tx-RIS}}} \tag{8}$$

where $\Phi_R \in \mathbb{C}^{M_R \times (Q+1)}$ and $\Phi_T \in \mathbb{C}^{(Q+1)\times M_T}$ respectively denote the receive and transmit slow-time varying phase response matrices of LoS and NLoS paths, $G = \text{diag}\{z_0/\sqrt{\alpha\tau_0^{\eta_0}}, z_1/\sqrt{\alpha\tau_1^{\eta}}, \ldots, z_Q/\sqrt{\alpha\tau_Q^{\eta}}\} \in \mathbb{C}^{(Q+1)\times(Q+1)}$ is the diagonal matrix represents the fast-time varying path gains. Here, the slow-time varying transmit and receive phase response matrices for the LoS and NLoS channels are defined as:

$$\Phi_T = \begin{bmatrix} \boldsymbol{a}_T^H\left(\gamma_{x,T}^{\text{LoS}}, \gamma_{y,T}^{\text{LoS}}\right) \\ \boldsymbol{a}_T^H\left(\gamma_{x,T}^{\text{NLoS},1}, \gamma_{y,T}^{\text{NLoS},1}\right) \\ \vdots \\ \boldsymbol{a}_T^H\left(\gamma_{x,T}^{\text{NLoS},Q}, \gamma_{y,T}^{\text{NLoS},Q}\right) \end{bmatrix}, \quad \Phi_R = \begin{bmatrix} \boldsymbol{a}_R^H\left(\gamma_{x,R}^{\text{LoS}}, \gamma_{y,R}^{\text{LoS}}\right) \\ \boldsymbol{a}_R^H\left(\gamma_{x,R}^{\text{NLoS},1}, \gamma_{y,R}^{\text{NLoS},1}\right) \\ \vdots \\ \boldsymbol{a}_R^H\left(\gamma_{x,R}^{\text{NLoS},Q}, \gamma_{y,R}^{\text{NLoS},Q}\right) \end{bmatrix}^H. \tag{9}$$

Then, the fast and slow-time varying components of the RIS-assisted sub-channels are defined as follows: $G_l =$

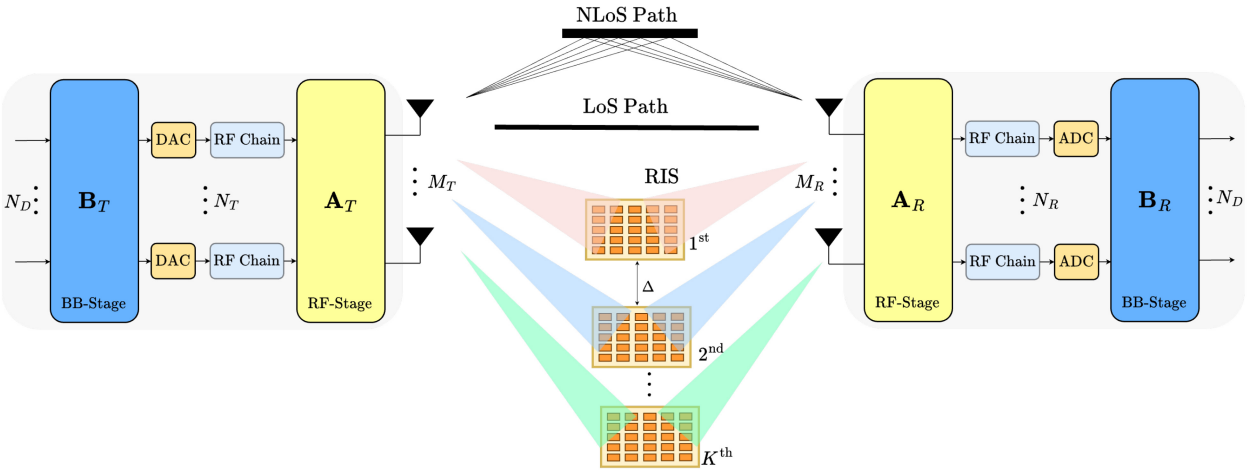


FIGURE 2. RIS-assisted hybrid mmWave massive MIMO system model.

$z_l/\sqrt{\alpha\tau_l^{n_0}}$, $\phi_R^l = \boldsymbol{a}_R^T(\gamma_{x,R}^l, \gamma_{y,R}^l)$, $\phi_T^l = \boldsymbol{a}_T^T(\gamma_{x,T}^l, \gamma_{y,T}^l)$ for $l \in$ {Tx-RIS, RIS-Rx}.

B. MULTI-RISS-AIDED TRANSMISSION

The utilization of multiple-RIS holds significant potential in terms of enhancing quality-of-service, improving reliability, and increasing flexibility in system design [20]. Efficiently transmitting multiple data streams along orthogonal paths poses a significant challenge in THz massive MIMO systems, particularly in scenarios where a reliable and dominant LoS channel exists between the Tx and Rx. To address this challenge, we investigate the potential of leveraging multiple-RIS in LoS dominant and sparse environments. By employing multiple-RIS, our objective is to transmit multiple data streams over different RIS-aided orthogonal paths, aiming to improve both the achievable rate performance and spatial multiplexing gain. In order to accomplish that goal, we utilize the multiple-RIS-assisted and NLoS paths during the transmission process by extending the single RIS-aided system model to the multiple-RIS case.

In order to extend the existing single RIS-aided system to a more advanced and versatile transmission scheme, we propose the utilization of multiple-RIS in the target communication system. An advanced hybrid THz massive MIMO architecture is proposed, leveraging the utilization of multiple-RIS in the transmission, as illustrated in Fig. 2. Each RIS consists of M_S reflecting elements, and we consider a total of K RISs in the setup. The proposed system in Fig. 2 positions each RIS unit in such a way to reduce direct interference by ensuring that each RIS operates within its designated spatial segment without overlapping footprints. To facilitate efficient signal propagation, both the Tx and Rx, along with the RISs, are equipped with half-wavelength spaced URA. Similar to the single RIS-aided system, the Tx and Rx are equipped with M_T and M_R antennas, respectively. As depicted in Fig. 2, the design ensures an appropriate alignment of the effective footprint area and the separation between RIS units (Δ) to prevent mutual interference[1] [30].

At the Tx, a sophisticated combination of the digital BB precoder B_T and analog RF beamformer A_T is employed to facilitate the transmission of N_D data streams, effectively utilizing N_T RF chains. On the receiving end, the received signal is skillfully processed through the analog RF beamformer A_R and digital BB combiner B_R, integrated with N_R RF chains. The presence of a constraint $N_D \leq \min\ (N_T, N_R)$ regulates the maximum number of data streams, ensuring optimal performance. Notably, the number of RF chains remains considerably smaller than the total number of transmit and receive antennas (i.e., $N_T \ll M_T$ and $N_R \ll M_R$), harnessing the inherent advantages offered by HBF systems. For simplicity, we will consider all parameters and methodologies in Tx and Rx units of the multiple-RIS system model the same as single RIS-aided transmission.

With the integration of multiple RIS, the data can now be transmitted over an expanded set of channels, encompassing the LoS and NLoS channels between the Tx and receiver Rx, as well as the channels assisted by the K RISs. Here, the LoS and NLoS channel between the Tx and Rx are respectively denoted by $H_{\text{LoS}} \in \mathbb{C}^{M_R \times M_T}$ and $H_{\text{NLoS}} \in \mathbb{C}^{M_R \times M_T}$, while each RIS-assisted link comprises two components: $H_{\text{Tx-RIS}}^k \in \mathbb{C}^{M_S \times M_T}$ represents the channel matrix from the Tx to the k^{th} RIS, and $H_{\text{Rx-RIS}}^k \in \mathbb{C}^{M_R \times M_S}$ represents the channel matrix from the k^{th} RIS to the Rx for $k \in \{1, 2, \ldots, K\}$. It should be noted that each subchannel here is modeled as in (5)-(7). Moreover, $\Theta_k = \text{diag}(e^{j\Omega_1^k}, \ldots, e^{j\Omega_{M_S}^k}) \in \mathbb{C}^{M_S \times M_S}$ corresponds to the phase reflection matrix of k^{th} RIS, where Ω_i^k denotes the phase shift introduced by the ith reflecting

[1]The practical deployment of multiple independent RIS units, as opposed to a single large-scale RIS, offers distinct advantages in minimizing unintended signal reflections. Employing a single large-scale RIS structured with sub-RIS segments interspersed with reflective elements would lead to unintended reflections from areas designated as non-reflective. As a result, this single large-scale RIS configuration could compromise system performance due to interference, as beam overspill from the effective footprint area would interact with additional reflective surfaces.

element of the k^{th} RIS for $i = 1, \ldots, M_S$ and $k = 1, \ldots, K$. Consequently, the received signal at the Rx incorporates contributions from the LoS, NLoS, and multiple-RIS-assisted paths. This can be mathematically expressed as

$$r = \underbrace{\left(H_{\text{LoS}} + H_{\text{NLoS}} + \sum_{k=1}^{K} H^k_{\text{RIS-Rx}} \Theta_k H^k_{\text{Tx-RIS}}\right)}_{H_K \in \mathbb{C}^{M_R \times M_T}} A_T B_T x + n, \tag{10}$$

where H_K stands for the end-to-end channel matrix of the multiple-RIS-aided system, while $n \sim \mathcal{CN}(0, \sigma_n^2 I_{M_R})$ denotes the complex Gaussian noise vector.

By following the similar steps with the single-RIS-aided system, with $\boldsymbol{\mathcal{H}}_K = A_R H A_T \in \mathbb{C}^{N_R \times N_T}$ being the effective channel matrix seen from the BB stages, the combined signal after the digital BB combiner is expressed as

$$\tilde{r} = B_R \boldsymbol{\mathcal{H}}_K B_T x + B_R A_R N, \tag{11}$$

where $A_R \in \mathbb{C}^{N_R \times M_T}$ and $B_R \in \mathbb{C}^{N_D \times N_R}$ denotes the receive RF beamformer and the BB combiner, respectively.

Here, we still aim to maximize the achievable rate of the system by carefully designing A_T, A_T, A_R, B_R and $\Theta_{\mathcal{S}} = \{\Theta_1, \ldots, \Theta_K\}$. Then, the multiple-RIS-aided AB-HBF design can be formulated as the following optimization problem:

$$\max_{\{A_T, A_R, B_T, B_R, \Theta_{\mathcal{S}}\}} \quad R = \log_2 \det\left(I_{N_D} + R_v^{-1} \tilde{\boldsymbol{\mathcal{H}}}_K \tilde{\boldsymbol{\mathcal{H}}}_K^H\right) \tag{12a}$$

$$\text{s.t. } \tilde{\boldsymbol{\mathcal{H}}}_K = B_R \boldsymbol{\mathcal{H}}_K B_T \in \mathbb{C}^{M_R \times M_T}, \tag{12b}$$

$$\boldsymbol{\mathcal{H}}_K = A_R H_K A_T \in \mathbb{C}^{N_R \times N_T}, \tag{12c}$$

$$|A_T(i,j)| = \frac{1}{\sqrt{M_T}}, \forall (i,j), \tag{12d}$$

$$|A_R(i,j)| = \frac{1}{\sqrt{M_R}}, \forall (i,j), \tag{12e}$$

$$\mathbb{E}\left\{\|\tilde{\mathbf{x}}\|_2^2\right\} = \text{tr}\left(B_T^H A_T^H A_T B_T\right) \leq P_{T_x}. \tag{12f}$$

The covariance matrix of the noise $v = B_r F_r n$ is denoted as $R_v = \sigma_n^2 B_R A_R A_R^H B_R^H$. Similar to the single RIS-aided case, the constraint of the constant module is ensured as expressed in (12e) due to the utilization of phase shifters.

Similar to (8), in order to obtain decomposed slow and fast time-varying components of each subchannel, the end-to-end channel H_K can be rewritten as

$$H_K = \underbrace{\Phi_R G \Phi_T}_{H_{\text{LoS}} + H_{\text{NLoS}}} + \sum_{k=1}^{K} \underbrace{\phi^{\text{RIS-Rx}}_{R,k} G^k_{\text{RIS-Rx}} \phi^{\text{RIS-Rx}}_{T,k}}_{H^k_{\text{RIS-Rx}}} \Theta_k \underbrace{\phi^{\text{Tx-RIS}}_{R,k} G^k_{\text{Tx-RIS}} \phi^{\text{Tx-RIS}}_{T,k}}_{H^k_{\text{Tx-RIS}}} \tag{13}$$

where $\Phi_R \in \mathbb{C}^{M_R \times (Q+1)}$ and $\Phi_T \in \mathbb{C}^{(Q+1) \times M_T}$ respectively denote the receive and transmit slow-time varying phase response matrices of LoS and NLoS paths defined in (9), $G = \text{diag}\{z_0/\sqrt{\alpha \tau_0^{\eta_0}}, z_1/\sqrt{\alpha \tau_1^{\eta}}, \ldots, z_Q/\sqrt{\alpha \tau_Q^{\eta}}\} \in \mathbb{C}^{(Q+1)\times(Q+1)}$ is the diagonal matrix represents the fast-time varying path gains. Here, the fast and slow-time varying components of the sub-channels aided by the kth RIS ($k = 1, \ldots, K$) are subsequently defined as $G_l^k = z_l^k/\sqrt{\alpha \tau_{l,k}^{n_0}}$, $\phi_R^{l,k} = \boldsymbol{a}_R^T(\gamma_{x,R}^{l,k}, \gamma_{y,R}^{l,k})$, $\phi_{T,k}^l = \boldsymbol{a}_T^T(\gamma_{x,T}^{l,k}, \gamma_{y,T}^{l,k})$ for $l \in \{\text{Tx-RIS}, \text{RIS-Rx}\}$ and $k \in \{1, \ldots, K\}$.

III. ANGULAR-BASED HYBRID BEAMFORMING DESIGN FOR RIS-AIDED THZ SYSTEMS

In this section, we present the design of RF beamformers, BB precoder/combiner, and phase shift matrices of the RISs for the proposed RIS-aided AB-HBF system in the THz band. Our main objective is to maximize the system's achievable rate while simultaneously reducing the size of CSI overhead and hardware complexity. Considering the extension to multiple-RIS-aided transmission, we provide a generalized approach that is applicable to both single and multiple RIS cases since multiple RIS transmission will be equivalent to single RIS transmission for $K = 1$.

In order to achieve our targets, the design procedures for the RF beamformers are provided based on the slow-time varying angular parameters in the THz band channel conditions. Then, the BB precoder/combiner is designed via the singular value decomposition (SVD) and water filling algorithm using the reduced-size effective channel. Finally, the phase shifts of the RIS are optimized using the PSO method, aiming to maximize the capacity of the system. By integrating these aforementioned design techniques and their benefits, we enhance the achievable rate of the system while alleviating the complexity associated with acquiring and processing CSI. Additionally, the proposed methodology is easily extended to scenarios involving multiple RIS, enabling the optimization of phase shift matrices for each RIS. This comprehensive approach enables the effective utilization of RISs in THz-based AB-HBF systems, leading to improved performance and reduced CSI overhead.

A. RF-STAGE DESIGN

The construction of the analog RF beamformer involves the deliberate focusing of signal energy in the desired direction, performed by exploiting the slow-time varying AoA/AoD information. To achieve an efficient design of the RF-stage, it is necessary to accurately define the range of azimuth and elevation AoA/AoD angles for the existing paths within the clusters, as outlined in [19], [31]. Therefore, AoA and AoD supports are obtained using (5) as:

$$\Upsilon_{\text{A}} = \left\{\left[\gamma_x, \gamma_y\right] = \sin(\theta)[\cos(\psi), \sin(\psi)] \middle| \theta \in \boldsymbol{\theta}_R, \psi \in \boldsymbol{\psi}_R\right\} \tag{14a}$$

$$\Upsilon_{\text{D}} = \left\{\left[\gamma_x, \gamma_y\right] = \sin(\theta)[\cos(\psi), \sin(\psi)] \middle| \theta \in \boldsymbol{\theta}_T, \psi \in \boldsymbol{\psi}_T\right\} \tag{14b}$$

where $\boldsymbol{\theta}_R = \boldsymbol{\theta}_R^{\text{Tx-RIS}} \cup \boldsymbol{\theta}_R^{\text{NLoS}} \cup \theta_R^{\text{LoS}}$, $\boldsymbol{\psi}_R = \boldsymbol{\psi}_R^{\text{Tx-RIS}} \cup \boldsymbol{\psi}_R^{\text{NLoS}} \cup \psi_R^{\text{LoS}}$, $\boldsymbol{\theta}_T = \boldsymbol{\theta}_T^{\text{RIS-Rx}} \cup \boldsymbol{\theta}_T^{\text{NLoS}} \cup \theta_T^{\text{LoS}}$, and $\boldsymbol{\psi}_T = \boldsymbol{\psi}_T^{\text{RIS-Rx}} \cup \boldsymbol{\psi}_T^{\text{NLoS}} \cup \theta_T^{\text{LoS}}$. Here, the elevation and azimuth AoA/AoD supports for the NLoS channel are respectively expressed

as: $\boldsymbol{\theta}_l^{\text{NLoS}} = \cup_{q=1}^{\mathcal{Q}}[\theta_{l,q}^{\text{NLoS}} - \delta_{l,q}^{\text{NLoS},\theta}, \theta_{l,q}^{\text{NLoS}} + \delta_{l,q}^{\text{NLoS},\theta}]$ and $\boldsymbol{\psi}_l^{\text{NLoS}} = \cup_{q=1}^{\mathcal{Q}}[\psi_{l,q}^{\text{NLoS}} - \delta_{l,q}^{\text{NLoS},\psi}, \psi_{l,q}^{\text{NLoS}} + \delta_{l,q}^{\text{NLoS},\psi}]$ for $l \in \{T, R\}$. Furthermore, the elevation and azimuth AoA/AoD supports for the RISs-assisted channels are respectively defined as $\boldsymbol{\theta}_l^j = \cup_{k=1}^{K}\theta_l^j$ and $\boldsymbol{\psi}_l^j = \cup_{k=1}^{K}\psi_l^j$ for $l \in \{T, R\}$ and $j \in \{\text{Tx-RIS}, \text{RIS-Rx}\}$.

By using (12c) and (13), the effective channel seen from the BB-stages can be rewritten as:

$$\begin{aligned}\boldsymbol{\mathcal{H}}_K &= A_R H_K A_T, \\ &= A_R\Big(\sum_{k=1}^{K}\phi_{R,k}^{\text{RIS-Rx}} G_{\text{RIS-Rx}}^k \phi_{T,k}^{\text{RIS-Rx}\Theta} k \phi_{R,k}^{\text{Tx-RIS}} G_{\text{Tx-RIS}}^k \phi_{T,k}^{\text{Tx-RIS}} \\ &\quad + \Phi_R G \Phi_T\Big) A_T. \end{aligned} \tag{15}$$

To fully leverage the available degrees of freedom offered by the channel and maximize the beamforming gain during transmission (reception), it is necessary for the columns of A_T (A_R) to reside within the subspace spanned by $\phi_T^{\text{Tx-RIS}}$ and Φ_T ($\phi_R^{\text{RIS-Rx}}$ and Φ_R). Therefore, the conditions as follows should be satisfied:

$$\begin{aligned}\text{Span}\ \ (A_T) &\subset \Big(\text{Span}\Big(\phi_T^{\text{Tx-RIS}}\Big) \cup \text{Span}(\Phi_T)\Big) \\ \text{Span}\ \ (A_R) &\subset \Big(\text{Span}\Big(\phi_R^{\text{RIS-Rx}}\Big) \cup \text{Span}(\Phi_R)\Big)\end{aligned} \tag{16}$$

Then, in order to construct the columns of the transmit RF beamformer matrix, the transmit steering vector is defined as

$$\begin{aligned}e_T(\gamma_x, \gamma_y) = \frac{1}{\sqrt{M_T}}\big[1, e^{j2\pi d\gamma_x}, \ldots, e^{j2\pi d(M_{T_x}-1)\gamma_x}\big]^T \\ \otimes\big[1, e^{j2\pi d\gamma_y}, \ldots, e^{j2\pi d\left(M_{T_y}-1\right)\gamma_y}\big]^T \in \mathbb{C}^{M_T}.\end{aligned} \tag{17}$$

By establishing the quantized angle-pairs as $\Lambda_{x,T}^i = \frac{2i-1}{M_{T_x}} - 1$ for $i = 1, \ldots, M_{T_x}$ and $\Lambda_{y,T}^j = \frac{2j-1}{M_{T_y}} - 1$ for $j = 1, \ldots, M_{T_y}$, we obtain a set of M_T orthogonal transmit steering vectors. These vectors represent the minimum required number of angle-pairs to encompass the entire elevation and azimuth space [15]. Hence, aiming to minimize the utilization of the RF chain while encompassing the complete AoD support, we express the quantized angle pairs within the AoD support as follows:

$$\Big(\Lambda_{x,T}^i, \Lambda_{y,T}^j\Big) \ \Big|\ \gamma_x \in \boldsymbol{\Lambda}_{x,T}^i, \gamma_y \in \boldsymbol{\Lambda}_{y,T}^j, (\gamma_x, \gamma_y) \in \Upsilon_{\text{D}}, \tag{18}$$

where the boundary of $\Lambda_{x,T}^i$ and $\Lambda_{y,T}^j$ are denoted as $\boldsymbol{\Lambda}_{x,T}^i = [\Lambda_{x,T}^i - \frac{1}{M_{T_x}}, \Lambda_{x,T}^i + \frac{1}{M_{T_x}}]$ and $\boldsymbol{\Lambda}_{y,T}^j = [\Lambda_{y,T}^j - \frac{1}{M_{T_y}}, \Lambda_{y,T}^j + \frac{1}{M_{T_y}}]$, respectively.

Based on (14b) and (21), the transmit RF beamformer is obtained as:

$$A_T = \big[e_T\big(\Lambda_{x,T}^{i_1}, \Lambda_{y,T}^{j_1}\big), \ldots, e_T\big(\Lambda_{x,T}^{i_{N_T}}, \Lambda_{y,T}^{j_{N_T}}\big)\big] \in \mathbb{C}^{M_T \times N_T}. \tag{19}$$

where N_T stands for the number of quantized angle pairs for AoD.

By employing a similar methodology, the receive RF beamformer, A_R, is devised based on the receive steering vector defined as

$$\begin{aligned}e_R(\gamma_x, \gamma_y) = \frac{1}{\sqrt{M_R}}\big[1, e^{j2\pi d\gamma_x}, \ldots, e^{j2\pi d(M_{R_x}-1)\gamma_x}\big]^T \\ \otimes\big[1, e^{j2\pi d\gamma_y}, \ldots, e^{j2\pi d\left(M_{R_y}-1\right)\gamma_y}\big]^T \in \mathbb{C}^{M_R}.\end{aligned} \tag{20}$$

The quantized angle-pairs are defined as $\Lambda_{x,R}^i = \frac{2i-1}{M_{R_x}} - 1$ for $i = 1, \ldots, M_{R_x}$ and $\Lambda_{y,R}^j = \frac{2j-1}{M_{R_y}} - 1$ for $j = 1, \ldots, M_{R_y}$. Using (14a), the quantized angle-pairs encompassing the AoA support can be expressed as

$$\Big(\Lambda_{x,R}^i, \Lambda_{y,R}^j\Big) \ \Big|\ \gamma_x \in \boldsymbol{\Lambda}_{x,R}^i, \gamma_y \in \boldsymbol{\Lambda}_{y,R}^j, (\gamma_x, \gamma_y) \in \Upsilon_{\text{A}}, \tag{21}$$

where $\boldsymbol{\Lambda}_{x,R}^i = [\Lambda_{x,R}^j - \frac{1}{M_{R_x}}, \Lambda_{x,R}^i + \frac{1}{M_{R_x}}]$ and $\boldsymbol{\Lambda}_{y,R}^j = [\Lambda_{y,R}^j - \frac{1}{M_{R_y}}, \Lambda_{y,R}^j + \frac{1}{M_{R_y}}]$ respectively denote the boundary of $\Lambda_{x,R}^i$ and $\Lambda_{y,R}^j$.

Incorporating equations (14a) and (21), the receive RF beamformer, comprising N_R quantized angle-pairs, is constructed as

$$A_R = \big[a_r\big(\Lambda_{x,r}^{m_1}, \Lambda_{y,r}^{n_1}\big), \ldots, e_T\big(\Lambda_{x,r}^{m_{N_R}}, \Lambda_{y,r}^{n_{N_R}}\big)\big] \in \mathbb{C}^{M_R \times N_R}. \tag{22}$$

It is noteworthy to emphasize that both the derived A_T and A_R adhere to the constant modulus property, as defined in (4d). Furthermore, A_T and A_R^H are tall unitary matrices, thereby yielding $A_T^H A_T = I_{N_T}$ and $A_R A_R^H = I_{N_R}$.

B. BASEBAND STAGE DESIGN

Following the RF beamformer design, we provide the design methodology of the BB precoder/combiner in this section, utilizing the low-dimensional effective channel matrix as described in (15). The effective channel matrix is subjected to singular value decomposition (SVD), resulting in the expression $\boldsymbol{\mathcal{H}}_K = U_K \Sigma_K V_K{}^H$, where $U_K \in \mathbb{C}^{N_R \times \text{rank}(\boldsymbol{\mathcal{H}}_K)}$ is a tall unitary matrix, $\Sigma_K = \text{diag}(\sigma_1^2, \ldots, \sigma_{\text{rank}(\boldsymbol{\mathcal{H}}_K)}^2) \in \mathbb{R}^{\text{rank}(\boldsymbol{\mathcal{H}}_K) \times \text{rank}(\boldsymbol{\mathcal{H}}_K)}$ stands for a diagonal matrix of singular values arranged in descending order, and $V_K \in \mathbb{C}^{N_T \times \text{rank}(\boldsymbol{\mathcal{H}}_K)}$ denotes another tall unitary matrix. Moreover, it is possible to partition matrix V_K as $V_K = [V_K^1, V_K^2]$ for $V_K^1 \in \mathbb{C}^{N_T \times N_D}$ by satisfying $N_D \leq \text{rank}(\boldsymbol{\mathcal{H}}_K)$.

Following a similar approach as in [14], [31]. The optimal solution for the BB precoder can then be expressed as

$$B_T = V_K^1 \Pi^{\frac{1}{2}} \in \mathbb{C}^{N_T \times N_T}, \tag{23}$$

where $\Pi = \text{diag}(\Pi_1, \ldots, \Pi_{N_D}) \in \mathbb{R}^{N_D \times N_D}$ represents a transmit power matrix with $\sum_{n=1}^{N_D}\Pi_n = P_{T_x}$ for meeting the power constraint given in (12f). Employing the water-filling power control solution [12], the power allocation is performed as:

$$\Pi_i = \left(\mu - \frac{\sigma_n^2}{P_{T_x}\sigma_i^2}\right)^+, \ \text{s.t.} \sum_{i=1}^{N_D}\left(\mu - \frac{\sigma_n^2}{P_{T_x}\sigma_i^2}\right)^+ = P_{T_x}. \tag{24}$$

where $\Pi = \text{diag}(\Pi_1, \ldots, \Pi_{N_D}) \in \mathbb{R}^{N_D \times N_D}$ denotes a transmit power matrix incorporating $\sum_{n=1}^{N_D} \Pi_n = P_{T_x}$ to satisfy the power constraint given in equation (12f).

Next, considering the provided RF beamformer (A_T/A_R), phase response matrix (Θ), and BB precoder (B_T), our objective is to design the BB combiner (B_R) that minimizes the mean-square error (MSE) between the transmitted and processed received signals. Referring to (11), the expression for MSE can be formulated as

$$\begin{aligned}\epsilon_{\text{MSE}} &= \mathbb{E}\{\|\tilde{r} - x\|^2\} = \text{tr}\big(\mathbb{E}\{\tilde{r}\tilde{r}^H - x\tilde{r}^H - \tilde{r}x^H + xx^H\}\big) \\ &= \text{tr}\big(\text{B}_\text{R}\boldsymbol{\mathcal{H}}_\text{K}\text{B}_\text{T}\text{B}_\text{T}^\text{H}\boldsymbol{\mathcal{H}}_\text{K}^\text{H}\text{B}_\text{R}^\text{H} - \text{B}_\text{R}\boldsymbol{\mathcal{H}}_\text{K}\text{B}_\text{T} - \text{B}_\text{T}^\text{H}\boldsymbol{\mathcal{H}}_\text{K}^\text{H}\text{B}_\text{R}^\text{H} + \text{I}_{\text{N}_\text{D}}\big).\end{aligned} \tag{25}$$

In order to determine the optimal solution for (25), the differentiation rules pertaining to complex-valid matrices are applied, resulting in the derivative of ϵ_{MSE} with respect to the BB combiner (B_R) is obtained as

$$\frac{\partial \epsilon_{\text{MSE}}}{\partial B_R} = 2B_R\boldsymbol{\mathcal{H}}_K B_T B_T^H \boldsymbol{\mathcal{H}}_K^H - 2B_T^H \boldsymbol{\mathcal{H}}_K^H. \tag{26}$$

Ultimately, the BB combiner that satisfies the minimum MSE criterion outlined in equation (25) can be obtained according to the following formulation:

$$B_R = B_T^H \boldsymbol{\mathcal{H}}_K^H \Big(\boldsymbol{\mathcal{H}}_K B_T B_T^H \boldsymbol{\mathcal{H}}_K^H\Big)^{-1}. \tag{27}$$

C. RIS PHASE SHIFT DESIGN

In this subsection, we provide the adjustment strategy of phase shifts in the RIS elements, aiming to maximize the achievable rate of the system through the utilization of the PSO algorithm. In PSO, each particle undergoes continuous repositioning within a multidimensional space, drawing upon its own experiences as well as the collective knowledge of its peers, all in pursuit of an optimal solution for the entire swarm [19], [32]. It is important to clarify that our methodology primarily utilizes separate CSI for RIS, which is critical for the precise design of the phase reflection matrix. This approach entails obtaining distinct channel information between the Tx and RIS, and between RIS and the Rx, enabling detailed control and dynamic optimization of RIS elements to significantly enhance signal propagation and improve overall system performance in the THz band.

After designing the transmit/receive RF beamformers (A_T, A_R) and BB precoder/combiner (B_T, B_R), the optimization problem given in (12a) can be reformulated as:

$$\begin{aligned}\max_{\{\Theta_1,\ldots,\Theta_K\}} \quad & R(A_T, A_R, B_T, B_R, \Theta_G) \\ \text{s.t.} \quad & \Theta_G = \text{diag}\Big(e^{j\Omega_1^1}, \ldots, e^{j\Omega_{M_S}^1}, e^{j\Omega_1^2}, \ldots, e^{j\Omega_{M_S}^K}\Big) \\ & \mathbb{E}\{\|x\|_2^2\} = \text{tr}\Big(B_T^H A_T^H A_T B_T\Big) \le P_{T_x} \\ & \Omega_i^k \in [0, 2\pi], \forall i, \forall k\end{aligned} \tag{28}$$

where $R(A_T, A_R, B_T, B_R, \Theta_G)$ is achievable rate expression defined in (12a). Here, Θ_G represents the global phase shift matrix, which captures the phase shifts of all elements across K RISs. It encompasses the collective phase adjustments applied to the elements of the RISs, resulting in a unified representation of the system's phase shift configuration.

In our PSO approach, we model the phase shifts of the RIS elements (Ω_i^k, $i \in \{1, \ldots, M_S\}$ and $k \in \{1, \ldots, K\}$) as the positions of the particles. The fitness function of the PSO algorithm is defined by the objective function presented in (28). Our PSO-based phase adjustment algorithm first initialize N_P particles with random positions $p \in \mathbb{C}^{KM_S}$ and velocities $v \in \mathbb{C}^{KM_S}$. Then, each particle maintains a record of its local best position ($p_{\text{best},i}^{(l)}$) and the global best position ($p_G^{(l)}$), which are determined based on the evaluation of the fitness function. Specifically, $p_{\text{best},i}^{(l)}$ represents the best position achieved by the i^{th} particle, while $p_G^{(l)}$ represents the best position achieved by any particle in the entire swarm during the l^{th} iteration.

At each iteration, the velocity and position of each particle are updated using the following equations:

$$v_i^{(l+1)} = \zeta v_i^{(l)} + \mu_1\rho_1\big(p_{\text{best},i}^{(l)} - p_i^{(l)}\big) + \mu_2\rho_2\big(p_G^{(l)} - p_i^{(l)}\big), \tag{29}$$

$$p_i^{(l+1)} = v_i^{(l+1)} + p_i^{(l)}, \tag{30}$$

where ζ represents the inertial weight of velocity, ρ_1 and ρ_2 are acceleration constants, and μ_1 and μ_2 are uniformly distributed random numbers within the range $[0, 1]$. As the iterations progress, the particles move from their current positions $p_i^{(l)}$ to the updated positions $p_i^{(l+1)}$. By considering the objective function in (28), the personal and the global best solutions for i^{th} particle at l^{th} iteration are expressed as:

$$p_{\text{best},i}^{(l)} = \underset{p_i^{(l^*)}, \forall l=0,1,\ldots,l}{\arg\max} \quad R\Big(A_T, A_R, B_T, B_R, p_i^{(l^*)}\Big) \tag{31}$$

$$p_{\text{best}}^{(l)} = \underset{p_{\text{best},i}^{(l^*)}, \forall i=0,1,\ldots,N_\text{P}}{\arg\max} \quad R\Big(A_T, A_R, B_T, B_R, p_{\text{best},i}^{(l)}\Big) \tag{32}$$

Finally, after L iterations, the RIS phase shift matrix is determined at the last iteration using a diagonal matrix representation: $\Theta_G = \text{diag}(\exp(jp_G^{(L)}))$. Algorithm 1 provides a comprehensive summary of the proposed RISs-aided AB-HBF system, which encompasses three stages of design, including our PSO solution for the phase adjustment process. The number of particles correlates with the breadth of the search space, affecting both the convergence speed and solution accuracy. Conversely, the number of iterations impacts the depth of the search, with more iterations allowing for thorough exploration but at the cost of increased computational time. To manage this complexity efficiently, our PSO implementation is designed to dynamically adjust these parameters based on the stability of channel conditions and the complexity of the environment, ensuring optimal performance without excessive computational demands.

The proposed RIS-aided AB-HBF technique introduces an efficient approach to construct the transmit and receive RF beamformers by utilizing only the AoD and AoA supports, as defined in (14a) and (14b), respectively. Subsequently, the BB precoder and combiner are developed according

Algorithm 1 Design Steps for the RIS-Aided AB-HBF System

Input: $\mathcal{H}_K$, Υ_A, Υ_D, P_{T_x}, L, N_P, ζ, ρ_1, ρ_2
Output: A_T, A_R, B_T, B_T, $\Theta_1,\ldots,\Theta_K$

Initialize the phase adjustments randomly for each matrix: $\Theta_k = \text{diag}\big(\exp\big(j2\pi(\text{randn}(1, M_S))\big)\big)$, $\forall k$.
Obtain A_T and A_R via (19) and (22), respectively.
Initialize N_P particles and their velocities
for $l = 1{:}L$ **do**
  Velocity of each particle $v_i^{(l)}$ is obtained as in (29).
  Position of each particle $p_i^{(l)}$ is obtained as in (30).
  Calculate B_T and B_R via (23) and (27), respectively.
  Find each particle's achievable rate via (28).
  Update personal best $p_{\text{best},i}^{(l)}$ and global best $p_G^{(l)}$.
end for
Set RIS phase-shift matrix as $\Theta_G = \text{diag}\big(\exp\big(jp_G^{(L)}\big)\big)$.
Build B_T and B_R as in (23) and (27) using the optimum phase shift matrix, respectively.

to (23) and (27), respectively. Furthermore, the phase shift matrices of the RISs are designed to maximize the achievable rate of the system and enhance the spatial multiplexing gain. When compared to the conventional fully digital precoding/combining (FDPC) approach, the proposed AB-HBF technique significantly reduces the required CSI overhead size and RF chain utilization.

In FDPC, the CSI overhead size is determined by a matrix with dimensions M_T by M_R. Thus, the CSI overhead size in FDPC is calculated as the multiplication of M_T and M_R as $M_T \times M_R$. Conversely, in AB-HBF, a reduced-dimensional representation of CSI is employed, resulting in the CSI overhead size being determined by $N_T \times N_R$.

In terms of the number of RF chains, FDPC requires M_T RF chains for the transmit antennas and M_R RF chains for the receive antennas. Consequently, the total number of RF chains in the FDPC system is obtained by $M_T + M_R$. On the other hand, AB-HBF utilizes N_T RF chains for the transmit antennas and N_R RF chains for the receive antennas, resulting in the total number of RF chains being $N_T + N_R$.

In the context of our RIS-aided THz massive MIMO system, efficient channel estimation can be facilitated by employing semi-passive RIS elements, which enable direct acquisition of the necessary CSI with minimal overhead [33]. This approach not only simplifies the channel estimation process but also provides a more accurate and timely reflection of the channel state, offering significant advantages in reducing the CSI overhead compared to traditional hybrid beamforming systems.

The channel estimation overhead for a system employing multiple RISs is inherently larger than that for a single RIS setup due to the increased number of channels to be estimated. Specifically, each RIS in a multiple-RIS configuration necessitates individual channel estimations for both its Tx-RIS and RIS-Rx links, proportionally increasing the overhead with the number of RISs used. This expansion in overhead must be carefully managed to harness the full potential of multiple RISs without incurring prohibitive estimation delays or resource consumption.

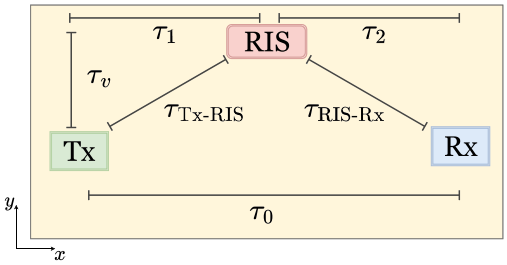


FIGURE 3. Top view of considered scenarios in simulations, illustrating the distances between terminals.

IV. NUMERICAL RESULTS

In this section, we provide a comprehensive analysis of the performance of the proposed RIS-empowered AB-HBF system in the THz massive MIMO system. We conduct extensive numerical simulations to evaluate the efficiency of the proposed system. Our another focus is on optimizing the phase shifts of the RIS using the PSO algorithm. The computer simulations are conducted based on a geometry-based THz channel model, which is described in (5). The separation between two antennas and reflectors is set to $d = 0.5$ to ensure a half-wavelength spacing. A schematic top-view representation of the simulation setup, including the distances between the terminals, is illustrated in Fig. 3.

A. FULLY-CONNECTED AB-HBF

In this subsection, we provide a comprehensive computer simulations by considering the traditional FC structure for RIS-aided AB-HBF system. Table 2 provides the common parameters utilized in the simulations. Scenario 1 is considered for the FC-AB-HBF system parameters in this subsection.

In Fig. 4, we investigate the achievable rate performance of the AB-HBF systems with or without RIS as a function of the transmit power P_{T_x}. Here, we aim to efficiently use the NLoS and RIS-assisted paths in the environment when the LoS link is blocked. We compare the proposed RIS-aided AB-HBF systems with an AB-HBF system that exclusively transmits data over LoS and NLoS channels. As clearly observed from Fig. 4, increasing P_{T_x} value improves the system performance for all schemes notably. Instead of using the NLoS path, only RIS-assisted transmission provides an improvement in achievable rate performance. Furthermore, the RIS and NLoS paths-assisted transmission substantially outperforms the NLoS path-aided transmission by providing additional paths for data transmission. Even if the LoS path does not exist, efficient usage of RIS and NLoS paths in the transmission provides to catch the performance of LoS conditions, especially for higher P_{T_x} values. As we observe, the utilization of the RIS-aided AB-HBF method offers the

TABLE 2. System parameters for simulations.

	Scenario 1	Scenario 2	Scenario 3
# of Tx antennas	$M_T = 64$	$M_T = 192$	$M_T = 16$
# of Rx antennas	$M_R = 64$	$M_R = 192$	$M_R = 16$
# of RIS elements	$M_S = 1024$	$M_S = 64$	$M_S = 64$
Frequency	100 GHz		
Channel Bandwidth	500 MHz		
Distances [m]	$\tau_0 = 10$, $\tau_1 = 1$, $\tau_2 = 9$, $\tau_q \in [10, 15]$		
# of paths	$Q = 10$ for $\mathbf{H}_{\text{NLoS}}$		
Path Loss	$\alpha = 32.4 + 20\log_{10}(f_c) = 72.4$, ($f_c$ [GHz])		
Noise PSD	-174 dBm/Hz		
PSO # of iterations	$L = 30$		
PSO # of particles	$N_{\text{P}} = 10$		
Path loss exponent	$\eta_0 = 2.1$ for LOS, $\eta = 4.5$ for NLOS		
Elevation AoA/AoD	$\theta_{i,q}^{\text{NLoS}} = 60°$, $\theta_i^{\text{LoS}} = 30°$, $i \in \{T, R\}$ $\theta_i^{\text{Tx-RIS}} = 60°$, $\theta_i^{\text{RIS-Rx}} = 50°$, $i \in \{T, R\}$		
Azimuth AoA/AoD	$\psi_{i,q}^{\text{NLoS}} = 120°$, $\psi_i^{\text{LoS}} = 60°$, $i \in \{T, R\}$ $\psi_i^{\text{Tx-RIS}} = 90°$, $\psi_i^{\text{RIS-Rx}} = 225°$, $i \in \{T, R\}$		

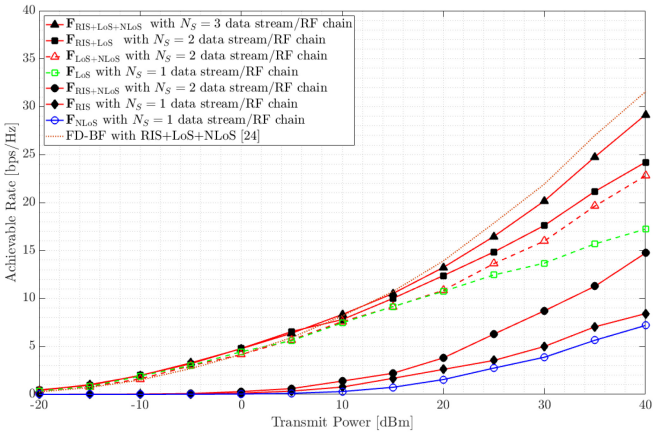


FIGURE 4. Achievable rate comparison for the proposed AB-HBF system with and without the TX-Rx link under changing P_{T_x}.

opportunity to convert a non-robust channel characterized by NLoS conditions into an LoS condition. This transformation is achieved by effectively leveraging the NLoS paths and the paths assisted by the RIS. By optimizing the phase shifts of the RIS elements via the proposed PSO-based solution, we are able to enhance the performance of the system and mitigate the disruptive effects of the wireless propagation environment while reducing the CSI overhead. In Fig. 4, we also include the fully digital beamforming-based approach outlined in [24], where the approach combines fully digital beamforming at the Tx with analog beamforming at the RIS, allowing for an insightful performance comparison with our proposed methodology. When the LoS, NLoS, and RIS-aided links are available, our solution achieves a favorably competitive performance with fewer RF chains and reduced CSI overhead. This comparative analysis substantiates the efficacy of our system, demonstrating its capability to deliver high performance while simultaneously minimizing system complexity and operational costs.

In Fig. 5, we aim to investigate the impact of different propagation environments characterized by varying path loss exponents on the achievable rate performance of the AB-HBF systems. Fig. 5(a) presents the achievable rate performance when data is transmitted over the LoS, NLoS, and RIS-aided paths (R_{ALL}), while Fig. 5(b) focuses solely on the achievable rate performance when only LoS channel is available (R_{LoS}). Moreover, Fig. 5(c) illustrates the difference in achievable rate performance between the R_{ALL} and the R_{LoS} scenario. This comparison highlights the contribution and effectiveness of incorporating NLoS and RIS-assisted paths in enhancing the overall system performance for various propagation characteristics. As seen in Fig. 5(c), even in the perfect LoS conditions, the RIS-aided design can provide a significant contribution to the system performance. For a specific scenario where the LoS and NLoS path loss exponents are respectively set to $\eta_0 = 2$ and $\eta = 3$, the achievable rate difference is measured as 11 bps/Hz, which means the 63% performance enhancement is achieved by exploiting the RIS and NLoS paths in the environment. Furthermore, the findings depicted in Fig. 5(c) highlight the challenge of improving system performance solely through a single RIS when the LoS channel is highly dominant and the contributions from NLoS channels are comparatively weaker. This observation can be attributed to the predominant influence of LoS propagation in THz channels, which indicates the need to explore the utilization of multiple-RIS to achieve additional performance improvements. Through this analysis, we provide insights into how the AB-HBF systems can effectively utilize and exploit the available LoS and NLoS paths, optimizing their performance based on the specific path loss characteristics of the environment. These results can provide a guideline for designing and optimizing AB-HBF systems to achieve high data rates and reliable communications in various wireless scenarios.

In Fig. 6, we investigate the impact of using multiple-RIS on the achievable rate performance of the AB-HBF system in the presence of a LoS link between the Tx and Rx for $K = 4$. Here, each RIS is vertically stacked with a fixed elevation angle separation of 10°. Fig. 6 demonstrates that the RIS-empowered AB-HBF system offers a significant gain in P_{T_X} as 32 dB compared to the AB-HBF system operating in NLoS conditions. It is also observed that performance superior to LoS conditions is achieved even by using only multiple-RIS-aided channels in the transmission. Furthermore, using multiple-RIS-aided paths as well as LoS path provides 18 dB gain in P_{T_x} compared to AB-HBF systems that transmit only through LoS channels. For higher P_{T_x} values, incorporating NLoS channels in addition to RISs and LoS channels during transmission can effectively enhance the spatial multiplexing gain, resulting in significant increases in the achievable rate performance of the AB-HBF systems. The system exhibits heightened sensitivity

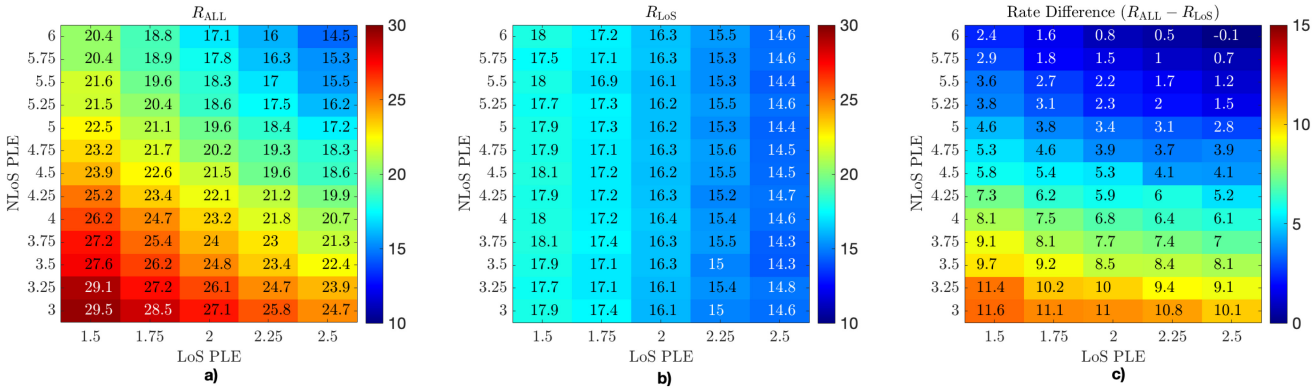


FIGURE 5. Achievable rate with varying path loss exponents for (a) LOS, NLOS, and RIS-assisted scenario (R_{ALL}), (b) considering only LoS path (R_{LoS}), and (c) difference in between R_{ALL} and R_{LoS}. The path loss exponent analysis investigates the impact of varying LoS and NLoS path loss exponents on the achievable rate of the AB-HBF system.

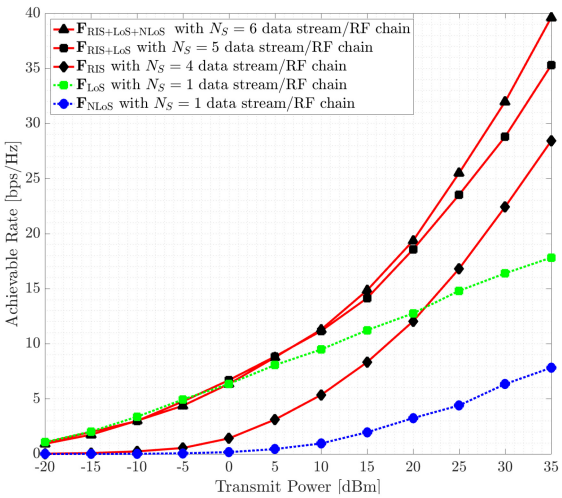


FIGURE 6. Achievable rate comparison for multiple-RIS-aided AB-HBF systems and AB-HBF for $K = 4$ under varying P_{T_x}.

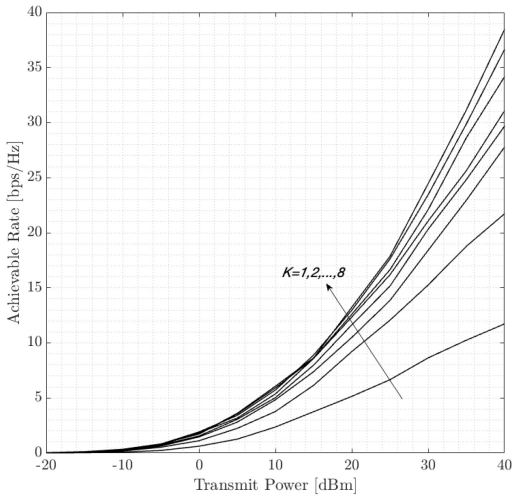


FIGURE 7. Effect of increasing K on achievable rate for multiple-RIS-aided AB-HBF systems under varying P_{T_x}.

to signal degradation in complex multi-path environments such as those involving RIS, LoS, and NLoS paths, leading to potentially counterintuitive performance outcomes due to the elevated interference and increased demands on signal processing associated with managing multiple simultaneous data streams. Additionally, while a single data stream/RF chain configuration in a pure LoS scenario demonstrates enhanced performance at lower power levels due to efficient direct path utilization, the advantages of employing RIS to support additional data streams become increasingly evident with rising transmit power, thereby substantially improving the system's capacity and performance.

Fig. 7 depicts the effect of increasing the number of RISs (K) on achievable rate performance of the multiple-RIS-empowered AB-HBF systems under varying P_{T_x}. Here, each RIS is vertically stacked with a fixed elevation angle separation of 5°. Each RIS is allocated for an independent data stream transmission, enabling concurrent transmission through multiple-RIS. As depicted in Fig. 7, the utilization of a greater number of RISs results in a significant improvement in the achievable rate performance. However, it is observed that the rate of performance enhancement diminishes as the number of RISs increases. The increasing slopes of achievable rate curves for each RIS further validate the spatial multiplexing gain achieved through multiple RIS. The incorporation of multiple-RIS in THz channels with limited scattering effectively enhances the rank of the channel matrix, thereby simulating an artificial rich-scattering environment. The effective utilization of multiple data streams over orthogonal links, which is one of the critical objectives of massive MIMO systems, can be achieved successfully in rich scattering environments. Consequently, the adoption of multiple-RIS emerges as a complementary technology to enhance the effectiveness of massive MIMO systems in THz channels. The use of multiple-RIS enables the exploitation of spatial multiplexing gain and facilitates the realization of the full potential of massive MIMO systems in THz frequency bands.

In Fig. 8, we present a detailed comparison of the PSO approach and a baseline random phase selection method

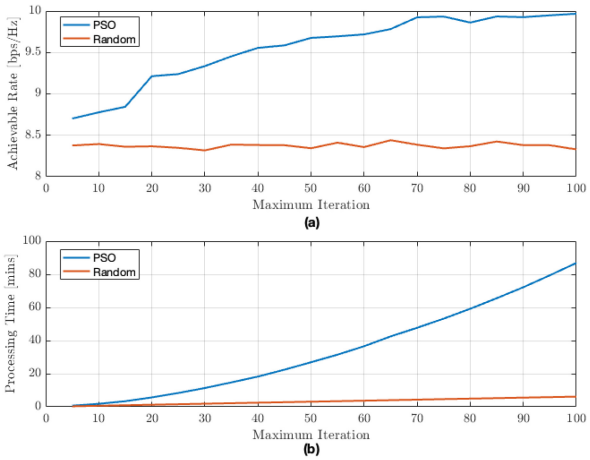


FIGURE 8. Comparison of (a) achievable rate and (b) processing time for PSO and random phase selection methods for increasing number of iterations.

across various iterations in order to address the convergence and computational efficacy of the PSO algorithm within our proposed framework. The results depicted in Fig. 8(a) demonstrate a distinct advantage of the PSO algorithm in enhancing the achievable rate, where a marked improvement is observed as the number of iterations increases, reaching a plateau phase beyond 80 iterations. This behavior not only confirms the convergence of the PSO algorithm but also showcases its ability to optimize system performance effectively. Furthermore, Fig. 8(b) provides insight into the computational demands associated with the PSO algorithm, illustrating a linear increase in processing time with the number of iterations. While the PSO algorithm incurs higher computational times compared to the random phase method, the significant gains in performance, as quantified by the achievable rate, substantiate the utility of this approach in scenarios demanding high optimization accuracy and system efficiency. From Fig. 8 it is also observed that with a configuration of 10 particles and 20 iterations, the computation time required was approximately 5.66 minutes on a PC equipped with an Intel Core i7-7700 CPU at 4.2 GHz and 32 GB of RAM, offering an achievable rate of 9.21 bps/Hz. When the number of iterations is increased to 90, the computation time is extended significantly to 72.17 minutes, while the achievable rate is improved to 9.92 bps/Hz. These results clearly illustrate the computational trade-offs involved in the optimization process, highlighting the critical balance between optimal system performance and efficient management of computational resources.

B. SUBARRAY-CONNECTED AB-HBF

In this subsection, we provide comparisons for the SC-AB-HBF system and FC-AB-HBF system to illustrate the trade-offs between these two use cases. For the numerical simulations in this subsection, we consider Scenario 2 from Table 2. Additionally, Fig. 3 provides a top view of the considered scenario in these simulations.

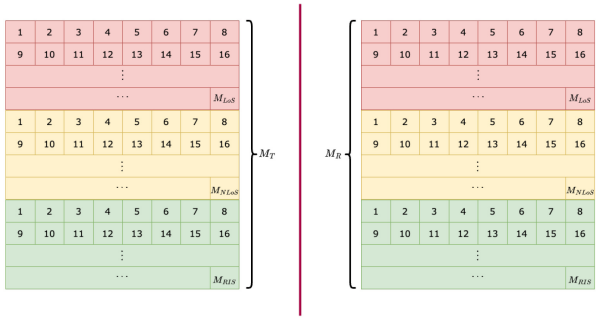


FIGURE 9. Transmit and receive antenna mappings for the SC-HBF structure considered scenarios in simulations.

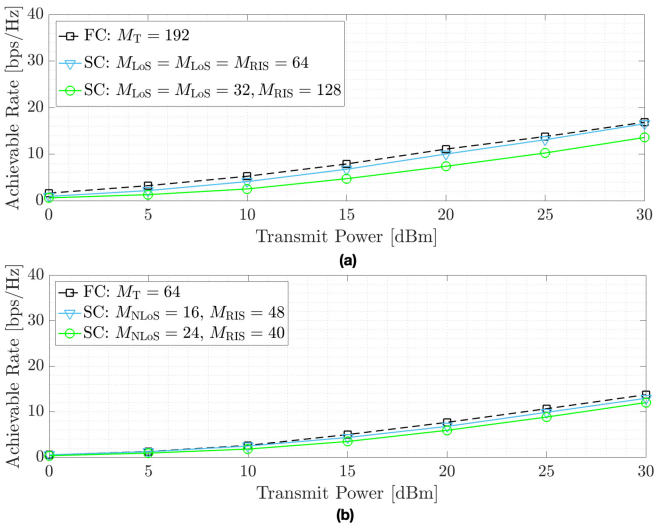


FIGURE 10. Performance comparisons of the FC and SC-AB-HBF Systems under different antenna configurations for (a) LoS, NLoS and RIS-aided, and (b) NLoS and RIS-aided transmission.

Fig. 9 illustrates the Tx/Rx antenna subarray configuration for the RIS-aided SC-AB-HBF system that is used for computer simulations. The Tx/Rx antennas are divided into three parts as M_{LoS}, M_{NLoS} and M_{RIS} representing different types of transmission paths associated with LoS, NLoS, and RISs, respectively. Each section specifies the distribution of antenna elements allocated for these specific paths. In Fig. 10, we provide a comparative performance analysis of multi-RIS-enabled FC and SC-AB-HBF methods for the THz mMIMO systems under $K = 3$. Fig. 10(a) investigates the RIS-assisted FC and SC-AB-HBF systems, encompassing three transmission paths: LoS, NLoS, and RIS-assisted paths while Fig. 10(b) compares the performance of the systems in scenarios including only NLoS and RIS-assisted paths. In Fig. 10(a), it is observed that if the number of resources allocated to the LoS path is increased for the SC-AB-HBF system, the achievable rate approaches that of the FC-AB-HBF system. In Fig. 10(b), it is seen that the performance of the SC-AB-HBF system approaches that of the FC-AB-HBF system by increasing the number of antennas allocated to the RIS-aided path. These observations demonstrate how

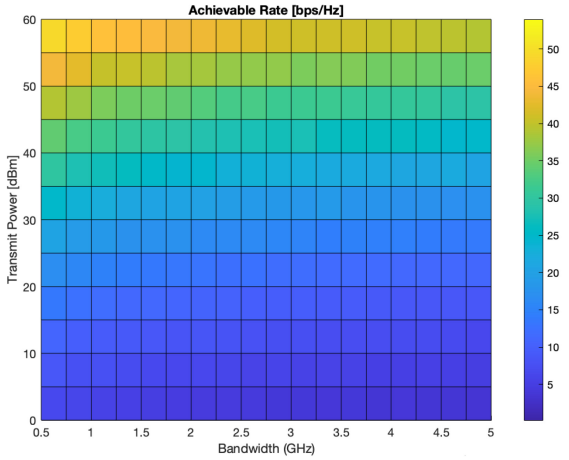


FIGURE 11. Achievable rate versus bandwidth and transmit power for the RIS and NLoS-aided transmission.

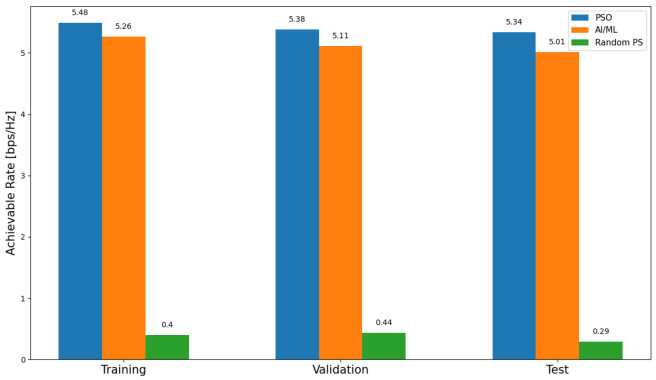


FIGURE 12. Comparison of achievable rates for PSO, DL, and random phase settings across training, validation, and test sets.

the adaptive mechanism in the system offers the flexibility needed to improve performance while reducing hardware costs. As a result, the SC-AB-HBF system exhibits a performance close to that of the FC-AB-HBF system, which stands out as a cost-effective solution. The graphs provide valuable information on how RIS-assisted AB-HBF systems can improve wireless communication performance under different antenna configurations and transmission powers.

It is noted that the total number of phase shifters is significantly reduced in the SC-AB-HBF compared to the FC-AB-HBF. For instance, considering $M_T = 192$ for FC-AB-HBF, with the assistance of AB-HBF and the use of $N_T = 14$ RF chains, the total number of phase shifters becomes $M_T \times N_T = 192 \times 14 = 2688$. On the other hand, for SC-AB-HBF, where $M_{LoS} = M_{NLoS} = M_{RIS} = 64$, the total number of phase shifters is reduced to $64 \times 14 = 960$. Thus, despite utilizing approximately one-third of the phase shifters, SC-AB-HBF and FC-AB-HBF exhibit comparable performance.

In Fig. 11, the relationship between the achievable rate, bandwidth, and transmit power is provided within a RIS and NLoS-aided transmission framework. It is evident that the achievable rate escalates in tandem with increases in bandwidth and transmit power, illustrating the system's adeptness at harnessing the expansive bandwidth characteristic of the THz band alongside augmented signal strength at elevated power levels. These findings compellingly demonstrate the scalable performance of RIS-aided systems operating in the THz band, thereby confirming their efficacy in facilitating high-rate communication in scenarios devoid of direct path connectivity. To ensure robust operation despite these challenges, our proposed designs presently assume a narrower operational bandwidth to maintain phase consistency across the frequency band. This approach simplifies the initial deployment of RIS technologies in THz systems but does not fully exploit the potential bandwidth available. We aim to develop advanced RIS configurations and control algorithms capable of adapting to the frequency-dependent characteristics of wideband signals in future implementations.

C. DEEP LEARNING-BASED PHASE SHIFT DESIGN

We have also implemented a supervised learning approach to optimize the RIS phases to reduce the processing time of the PSO-based phase shift design. Scenario 3 from Table II is considered for the simulations in this subsection. Initially, we generate a dataset through simulations of various RIS configurations, capturing effective channel responses and their corresponding achievable rates. This dataset is split into training, validation, and test sets to ensure comprehensive model evaluation.

The core of our approach involves constructing a CNN designed to predict optimal RIS phases. The model architecture includes two primary inputs representing different channel responses ($H_{\text{Tx-RIS}}$ and $H_{\text{RIS-Rx}}$). Each input is processed through separate residual blocks consisting of convolutional layers, batch normalization, and shortcut connections. The outputs from these blocks are concatenated and further refined through additional residual blocks. Finally, the output is flattened and passed through dense layers with a ReLU activation function, capped at 2π, to produce the predicted phase angles of the RIS.

In Fig. 12, the performance of the DL-based model is evaluated against the PSO method and random phase settings. As can be seen from Fig. 12, the DL-based approach achieves average achievable rates of 5.26 bps/Hz, 5.11 bps/Hz, and 5.01 bps/Hz for the training, validation, and test sets, respectively, which are very close to the rates achieved by PSO (5.40 bps/Hz, 5.38 bps/Hz, and 5.34 bps/Hz). In contrast, the random phase settings resulted in significantly lower rates (0.4 bps/Hz, 0.44 bps/Hz, and 0.29 bps/Hz), highlighting the effectiveness of our DL-based model. The proposed DL-based solution demonstrates a substantial time efficiency, achieving approximately a 95% reduction in processing time compared to the PSO-based solution under the same conditions. These results demonstrate that the DL-based model effectively learns the optimal RIS phase configurations, achieving performance comparable to the PSO method while offering a scalable and

efficient solution for real-time phase adjustment in practical scenarios. This approach enhances the performance of wireless communication systems, demonstrating the potential for advanced adaptive communication technologies.

V. CONCLUSION

This paper has presented an innovative approach for THz band communications by leveraging RISs in conjunction with an AB-HBF technique. The study has addressed two significant scenarios commonly encountered in THz channels and proposed cost and energy-efficient solutions utilizing RISs to enhance system performance. The first scenario focused on ensuring reliable communication in the presence of obstacles obstructing the direct path between the transmitter and receiver. By utilizing RISs as an alternative transmission path, reliable communication has been maintained. The second scenario explored the utilization of multiple-RIS in LoS dominant or sparse environments to increase the rank of the channel matrix, consequently improving the achievable rate performance. The incorporation of RIS in AB-HBF systems is primarily aimed at enhancing the channel's effective rank, particularly in scenarios where transmitting multiple data streams over a naturally low-rank channel is challenging. This strategic deployment of RIS not only facilitates high-throughput communications in adverse conditions but also does so with a cost structure that remains competitive when compared to more traditional, high-cost beamforming setups. Our analysis confirms that the additional equipment and control links required for RIS integration are justified by the significant improvements in channel quality and system capacity, making it a worthwhile investment in long-term system performance and reliability. We also demonstrate that the SC-AB-HBF configuration offers a remarkable reduction in the total number of phase shifters compared to the FC-AB-HBF. Extensive numerical experiments have demonstrated a significant enhancement in the achievable rate performance of THz AB-HBF systems through the incorporation of RISs. This approach has effectively mitigated the disruptive effects of the wireless propagation environment while reducing hardware cost/complexity and power consumption for massive MIMO systems with large antenna arrays. Overall, this research contributes to the advancement of THz band communications, offering efficient and high-performance solutions for overcoming transmission challenges and exploiting the potential of RIS-assisted AB-HBF techniques.

REFERENCES

[1] C. Chaccour, M. N. Soorki, W. Saad, M. Bennis, P. Popovski, and M. Debbah, "Seven defining features of terahertz (THz) wireless systems: A fellowship of communication and sensing," *IEEE Commun. Surveys Tuts.*, vol. 24, no. 2, pp. 967–993, 2nd Quart., 2022.

[2] W. Jiang, B. Han, M. A. Habibi, and H. D. Schotten, "The road towards 6G: A comprehensive survey," *IEEE Open J. Commun. Soc.*, vol. 2, pp. 334–366, 2021.

[3] Q. Yue, J. Hu, and K. Yang, "Low complexity but near optimal hybrid beamforming design in tera-hertz communication systems: Principles and opportunities," *Inst. Eng. Technol. Microw., Antennas Propagat.*, vol. 17, no. 8, pp. 595–603, 2023. [Online]. Available: https://ietresearch.onlinelibrary.wiley.com/doi/abs/10.1049/mia2.12383

[4] Z. Chen, X. Ma, C. Han, and Q. Wen, "Towards intelligent reflecting surface empowered 6G terahertz communications: A survey," *China Commun.*, vol. 18, no. 5, pp. 93–119, May 2021.

[5] C. Han, W. Gao, N. Yang, and J. M. Jornet, "Molecular absorption effect: A double-edged sword of terahertz communications," *IEEE Wireless Commun.*, vol. 30, no. 4, pp. 140–146, Aug. 2023.

[6] I. Yildirim, M. Mahmood, E. Basar, and T. Le-Ngoc, "Spider RIS: Mobilizing intelligent surfaces for enhanced wireless communications," in *Proc. Joint Eur. Conf. Netw. Commun. 6G Summit (EuCNC/6G Summit)*, Antwerp, Belgium, 2024, pp. 440–445.

[7] E. Basar and I. Yildirim, "Reconfigurable intelligent surfaces for future wireless networks: A channel modeling perspective," *IEEE Wireless Commun.*, vol. 28, no. 3, pp. 108–114, Jun. 2021.

[8] I. Yildirim, F. Kilinc, E. Basar, and G. C. Alexandropoulos, "Hybrid RIS-empowered reflection and decode-and-forward relaying for coverage extension," *IEEE Commun. Lett.*, vol. 25, no. 5, pp. 1692–1696, May 2021.

[9] E. Basar, M. Di Renzo, J. De Rosny, M. Debbah, M.-S. Alouini, and R. Zhang, "Wireless communications through reconfigurable intelligent surfaces," *IEEE Access*, vol. 7, pp. 116753–116773, 2019.

[10] E. G. Larsson, O. Edfors, F. Tufvesson, and T. L. Marzetta, "Massive MIMO for next-generation wireless systems," *IEEE Commun. Mag.*, vol. 52, no. 2, pp. 186–195, Feb. 2014.

[11] A. F. Molisch et al., "Hybrid beamforming for massive MIMO: A survey," *IEEE Commun. Mag.*, vol. 55, no. 9, pp. 134–141, Sep. 2017.

[12] F. Sohrabi and W. Yu, "Hybrid analog and digital beamforming for mmWave OFDM large-scale antenna arrays," *IEEE J. Sel. Areas Commun.*, vol. 35, no. 7, pp. 1432–1443, Jul. 2017.

[13] X. Yu, J.-C. Shen, J. Zhang, and K. B. Letaief, "Alternating minimization algorithms for hybrid precoding in millimeter wave MIMO systems," *IEEE J. Sel. Topics Signal Process*, vol. 10, no. 3, pp. 485–500, Apr. 2016.

[14] O. E. Ayach, S. Rajagopal, S. Abu-Surra, Z. Pi, and R. W. Heath, "Spatially sparse precoding in millimeter wave MIMO systems," *IEEE Trans. Wireless Commun.*, vol. 13, no. 3, pp. 1499–1513, Mar. 2014, doi: 10.1109/TWC.2014.011714.130846.

[15] A. Koc, A. Masmoudi, and T. Le-Ngoc, "3D angular-based hybrid precoding and user grouping for uniform rectangular arrays in massive MU-MIMO systems," *IEEE Access*, vol. 8, pp. 84689–84712, 2020.

[16] S. Park, A. Alkhateeb, and R. W. Heath, "Dynamic subarrays for hybrid precoding in wideband mmwave MIMO systems," *IEEE Trans. Wireless Commun.*, vol. 16, no. 5, pp. 2907–2920, May 2017.

[17] W. Zheng, A. Koc, and T. Le-Ngoc, "Sub-connected hybrid precoding architectures in massive MIMO systems," in *Proc. IEEE Global Commun. Conf. (GLOBECOM)*, Taipei, Taiwan, 2020, pp. 1–6.

[18] E. Basar, I. Yildirim, and F. Kilinc, "Indoor and outdoor physical channel modeling and efficient positioning for reconfigurable intelligent surfaces in mmWave bands," *IEEE Trans. Commun.*, vol. 69, no. 12, pp. 8600–8611, Dec. 2021.

[19] I. Yildirim, A. Koc, E. Basar, and T. Le-Ngoc, "RIS-aided angular-based hybrid beamforming design in mmWave massive MIMO systems," in *Proc. IEEE Global Commun. Conf. (GLOBECOM)*, Rio de Janeiro, Brazil, 2022, pp. 5267–5272.

[20] I. Yildirim, A. Uyrus, and E. Basar, "Modeling and analysis of reconfigurable intelligent surfaces for indoor and outdoor applications in future wireless networks," *IEEE Trans. Commun.*, vol. 69, no. 2, pp. 1290–1301, Feb. 2021.

[21] M. Jian, R. Liu, and Y. Zhao, "Spatial multiplexing optimization for RIS-assisted wireless communication using practical models," in *Proc. IEEE Global Commun. Conf. (GLOBECOM)*, Rio de Janeiro, Brazil, 2022, pp. 656–661.

[22] O. Ozdogan, E. Björnson, and E. G. Larsson, "Using intelligent reflecting surfaces for rank improvement in MIMO communications," in *Proc. IEEE ICASSP*, 2020, pp. 9160–9164.

[23] C. Huang et al., "Hybrid beamforming for RIS-empowered multi-hop terahertz communications: A DRL-based method," in *Proc. IEEE GLOBECOM Workshops (GC Wkshps)*, 2020, pp. 1–6.

[24] Y. Lu, M. Hao, and R. Mackenzie, "Reconfigurable intelligent surface based hybrid precoding for THz communications," *Intell. Converged Netw.*, vol. 3, no. 1, pp. 103–118, Mar. 2022.
[25] B. Ning, Z. Chen, W. Chen, Y. Du, and J. Fang, "Terahertz multi-user massive MIMO with intelligent reflecting surface: Beam training and hybrid beamforming," *IEEE Trans. Veh. Technol.*, vol. 70, no. 2, pp. 1376–1393, Feb. 2021.
[26] A. M. Elbir, K. V. Mishra, and S. Chatzinotas, "Terahertz-band joint ultra-massive MIMO radar-communications: Model-based and model-free hybrid beamforming," *IEEE J. Sel. Topics Signal Process*, vol. 15, no. 6, pp. 1468–1483, Nov. 2021.
[27] M. Shehab et al., "Terahertz multiple access: A deep reinforcement learning controlled multihop IRS topology," *IEEE Open J. Commun. Soc.*, vol. 5, pp. 1072–1087, 2024.
[28] S. Farrag, E. A. Maher, A. El-Mahdy, and F. Dressler, "Sum rate maximization of uplink active RIS and UAV-assisted THz mobile communications," in *Proc. 19th Int. Conf. Design Rel. Commun. Netw. (DRCN)*, 2023, pp. 1–7.
[29] A. Saleh and R. Valenzuela, "A statistical model for indoor multipath propagation," *IEEE J. Sel. Areas Commun.*, vol. 5, no. 2, pp. 128–137, Feb. 1987.
[30] M. Raeisi, I. Yildirim, M. C. Ilter, M. Gerami, and E. Basar, "Plug-in RIS: A novel approach to fully passive reconfigurable intelligent surfaces," *IEEE Trans. Wireless Commun.*, early access, Jul. 2, 2024, doi: 10.1109/TWC.2024.3418969.
[31] A. Koc and T. Le-Ngoc, "Hybrid millimeter-wave massive MIMO systems with low CSI overhead and few-bit DACs/ADCs," in *Proc. IEEE 92nd Veh. Technol. Conf. (VTC)*, 2020, pp. 1–5.
[32] W. Tong, A. Hussain, W. X. Bo, and S. Maharjan, "Artificial intelligence for vehicle-to-everything: A survey," *IEEE Access*, vol. 7, pp. 10823–10843, 2019.
[33] J. Hu, H. Yin, and E. Björnson, "MmWave MIMO communication with semi-passive RIS: A low-complexity channel estimation scheme," in *Proc. IEEE Global Commun. Conf. (GLOBECOM)*, 2021, pp. 1–6.